

Emergence of flat bands and their impact on superconductivity of $\text{Mo}_5\text{Si}_{3-x}\text{P}_x$

Rustem Khasanov^{1,*}, Bin-Bin Ruan^{2,†}, Yun-Qing Shi^{2,3}, Gen-Fu

Chen^{2,3}, Hubertus Luetkens¹, Zhi-An Ren^{2,3}, and Zurab Guguchia¹

Laboratory for Muon Spin Spectroscopy, Paul Scherrer Institut, CH-5232 Villigen PSI, Switzerland

Institute of Physics and Beijing National Laboratory for Condensed Matter Physics,

Chinese Academy of Sciences, Beijing 100190, China and

School of Physical Sciences, University of Chinese Academy of Sciences, Beijing 100049, China

The first-principles calculations and measurements of the magnetic penetration depths, the upper critical field, and the specific heat were performed for a family of $\text{Mo}_5\text{Si}_{3-x}\text{P}_x$ superconductors. First-principles calculations suggest the presence of a flat band dispersion, which gradually shifts to the Fermi level as a function of phosphorus doping x . The flat band approaches the Fermi level at $x \simeq 1.3$, thus separating $\text{Mo}_5\text{Si}_{3-x}\text{P}_x$ between the purely steep band and the steep band/flat band superconducting regimes. The emergence of flat bands lead to an abrupt change of nearly all the superconducting quantities. In particular, a strong reduction of the coherence length ξ and enhancement of the penetration depth λ result in nearly factor of three increase of the Ginzburg-Landau parameter $\kappa = \lambda/\xi$ (from $\kappa \simeq 25$ for $x \lesssim 1.2$ to $\kappa \simeq 70$ for $x \gtrsim 1.4$) thus initiating the transition of $\text{Mo}_5\text{Si}_{3-x}\text{P}_x$ from a moderate to an extreme type-II superconductivity.

Electrons with a narrow energy dispersion in the closed vicinity to the Fermi level are expected to demonstrate a broad variety of physics phenomena. Such electrons form a 'quasi-flat' bands, where the many-body effects dominate over the kinetic energy. The famous example of a flat band physics is the the fractional quantum hole effect, where the Hall conductance of 2-dimensional electrons shows precisely quantized plateaus at fractional values of e^2/h . The quasiparticle excitations appears under a fractional filling of an electronic flat band which develops in the presence of a large magnetic field.¹⁻⁴ Another example is the twisted bilayer graphene, where flat bands are formed already at zero magnetic fields.⁵ There, a flat electronic bands create large, many nanometre-size moiré unit cells, which folds and flattens the initial band structure of the material.⁶ Such flattening plays a crucial role in the physics of bilayer graphene and leads to appearance of a strong-coupling superconductivity, with the phase diagram resembling that of the high-temperature cuprates.^{5,7}

Both above mentioned examples correspond to a rare case where the bands at the Fermi level stay nearly flat. In reality, the situation with the 'quasi-flat' band is more often to be realised. This is not so rare as might be thought, however. The recent careful search performed by Regnault *et al.*,⁸ where more than 55 thousand compounds were analyzed, presented a catalogue of the naturally occurring three-dimensional stoichiometric materials with the quasi-flat bands around the Fermi level. It was found, in particular, that more than 5% of all searched materials host a flat band structures.

In relation to the superconducting materials, the importance of flat bands stems from substantial decrease of the Fermi velocity, which may even tend to zero in a true flat band case. Within the conventional Bardeen-Cooper-Schrieffer (BCS) approach this leads to a vanishingly small coherence length and the superfluid density, as well as to the extreme heavy and nearly immobile supercarriers. From the theory site, however,

the emergence of flat bands stay in a favor to superconductivity by giving rise to a linear dependence of the transition temperature on the strength of the attractive interactions.⁹⁻¹² More interesting, the coexistence of flat and dispersive bands within the multi-band scenario lead to a strong enhancement of the transition temperature and might potentially explain the phenomena of high-temperature superconductivity in cuprates and recently discovered hydride superconductors.¹³

In this work we probe the effect of band flattening on properties of $\text{Mo}_5\text{Si}_{3-x}\text{P}_x$ superconductors. The emergence of flat bands leads to an abrupt change of nearly all superconducting quantities including: the transition temperature T_c , the upper critical field H_{c2} , the magnetic penetration depth λ , the coherence length ξ and the superconducting energy gap Δ .

Polycrystalline $\text{Mo}_5\text{Si}_{3-x}\text{P}_x$ samples with $x = 0.5, 1.0, 1.2, 1.3, 1.4, 1.5,$ and 1.6 were prepared by a solid-state reaction method.¹⁴ In addition to the main $\text{Mo}_5\text{Si}_{3-x}\text{P}_x$ phase, a small amount of impurity phase Mo_3P (from $\simeq 5$ to 10%) was detected.¹⁵ The first-principles calculations were performed based on the density functional theory, as implemented in the Quantum ESPRESSO package.¹⁶ The superconducting properties were characterized by electrical resistivity and heat capacity measurements, performed on a Quantum Design PPMS (physical property measurement system). The muon-spin rotation/relaxation (μSR) measurements were carried out at the $\pi\text{M}3$ beam line by using GPS (General Purpose Surface) μSR spectrometer (Paul Scherrer Institut, Villigen, Switzerland).¹⁷ In this study, mostly the transverse-field (TF) μSR measurements were performed, which allowed to determine the temperature evolution of the magnetic penetration depth. The μSR data were analyzed by means of the Musrfit software package.¹⁸ The details of the sample preparation, the first-principles calculations, as well as the x-ray, resistivity, specific heat, and μSR experiments are provided in the Supplemental part.¹⁵

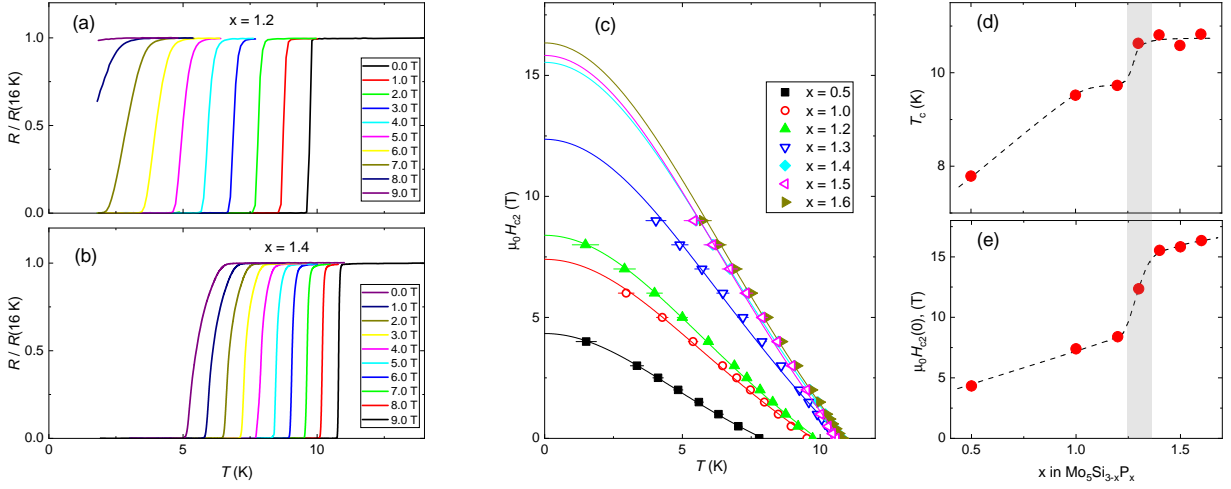


FIG. 1: (a) and (b) The temperature dependencies of resistivity of $\text{Mo}_5\text{Si}_{3-x}\text{P}_x$ ($x = 1.2$ and 1.4) samples measured in magnetic fields ranging from 0.0 to 9.0 T. (c) Temperature dependencies of the upper critical field H_{c2} . The lines are fits of Eq. 1 to the data. (d) Doping dependence of the transition temperature T_c . (e) Doping dependence of the zero-temperature value of the upper critical field $H_{c2}(0)$. The lines in (d) and (e) are guides for the eye. The grey stripe represents the region of an abrupt change of T_c and $H_{c2}(0)$.

The doping evolution of the upper critical field H_{c2} was studied by means of resistivity. Figures 1 (a) and (b) show the resistivity curves normalized to the values at $T = 16$ K [$R(T)/R(16\text{ K})$] measured in magnetic fields ranging from 0.0 to 9.0 T for two representative phosphorus dopings $x = 1.2$ and $x = 1.4$, respectively. Obviously, the two closely doped samples, which have nearly similar superconducting transition temperatures at zero applied field ($\mu_0 H_{\text{ap}} = 0.0$ T), reacts differently on the magnetic field. As an example, at $\mu_0 H_{\text{ap}} = 9.0$ T the $x = 1.2$ sample stays in a normal state down to $T \simeq 1.75$ K, while the $x = 1.4$ one superconducts below $\simeq 5$ K.

The upper critical field values defined from $R(T)$ measurement curves are summarized in Fig. 1 (c). Here, $T_c(H_{\text{ap}})$'s were determined from the mid point of $R(T, H_{\text{ap}})$ curves [*i.e.* as the value where $R(T)/R(16\text{ K}) = 0.5$]. The solid lines correspond to the fits of the Ginzburg-Landau model

$$H_{c2}(T) = H_{c2}(0) \frac{1 - (T/T_c)^2}{1 + (T/T_c)^2} \quad (1)$$

to the experimental $H_{c2}(T)$ data. The values of T_c 's at $H_{\text{ap}} = 0$ and $H_{c2}(0)$'s from fits of Eq. 1 are presented in Figs. 1 (d) and (e) as a function of phosphorus doping x . An abrupt change of both parameters at $x \simeq 1.3$ is clearly visible.

The temperature dependencies of the magnetic penetration depth λ were studied in TF- μ SR experiments. Measurements were performed in the field cooling mode at the applied field $\mu_0 H_{\text{ap}} = 50$ mT. Representative TF- μ SR time-spectra of $x = 1.2$ and 1.4 samples at $T \simeq 1.5$ K (*i.e.* below T_c) are shown in Figs. 2 (a) and (b). A strong damping reflects the inhomogeneous field distribution $P(B)$ caused by the formation of the flux-line lattice (FLL). The broad asymmetric distribution is clearly

visible in Figs. 2 (c) and (d), where the Fourier transform of the corresponding TF- μ SR data are shown. The $P(B)$ distributions demonstrate all characteristic features of a well arranged FLL, namely the cut-off at low-field, the extended tail to the higher field values and shift of the $P(B)$ peak below $\mu_0 H_{\text{ap}}$.¹⁹ Note that the narrow peak at the applied field position ($B_{\text{ap}} = \mu_0 H_{\text{ap}}$) originates from muons missing the sample.

The width of $P(B)$ within the FLL in the limit of $H_{\text{ap}} \ll H_{c2}$ [as is the case for our studies, see Figs. 1 (c) and (e)] is primarily determined by the value of the magnetic penetration depth λ .^{19–21} Comparison of $P(B)$'s presented in Figs. 2 (c) and (d) suggests that $x = 1.2$ sample has stronger broadening (*i.e.* smaller λ value) compared to that of $x = 1.4$ one. The analysis of TF- μ SR data was performed by considering the presence of a main $\text{Mo}_5\text{Si}_{3-x}\text{P}_x$ phase (denoted as 's') and two background contributions ('bg,1' and 'bg,2'), respectively. The 'bg,1' contribution originates from the impurity Mo_3P phase (which superconducts at $T_c \simeq 5.5$ K, Refs. 22–24), while the 'bg,2' one is caused by muons missing the sample (*i.e.* stopped at the sample holder and the cryostat windows). The following functional form was used:

$$A(t) = A_s \text{SkG}(t, B_s, \sigma_+, \sigma_-) + A_{\text{bg},1} e^{-\sigma_{\text{bg},1}^2 t^2 / 2} \cos(\gamma_\mu B_{\text{bg},1} + \phi) + A_{\text{bg},2} \cos(\gamma_\mu B_{\text{ap}} + \phi). \quad (2)$$

Here A_s ($\sim 90\%$), $A_{\text{bg},1}$ ($\sim 10\%$), and $A_{\text{bg},2}$ ($\sim 1\%$) are the initial asymmetries, and B_s , $B_{\text{bg},1}$, and B_{ap} are the internal fields of each particular component. $\gamma_\mu = 2\pi \cdot 135.53$ MHz/T is the muon gyromagnetic ratio, ϕ is the initial phase of the muon-spin ensemble, and σ is the Gaussian relaxation rate. The sample contribution was fitted with the Skewed Gaussian function [$\text{SkG}(B, \sigma_+, \sigma_-)$], which accounts for the asymmet-

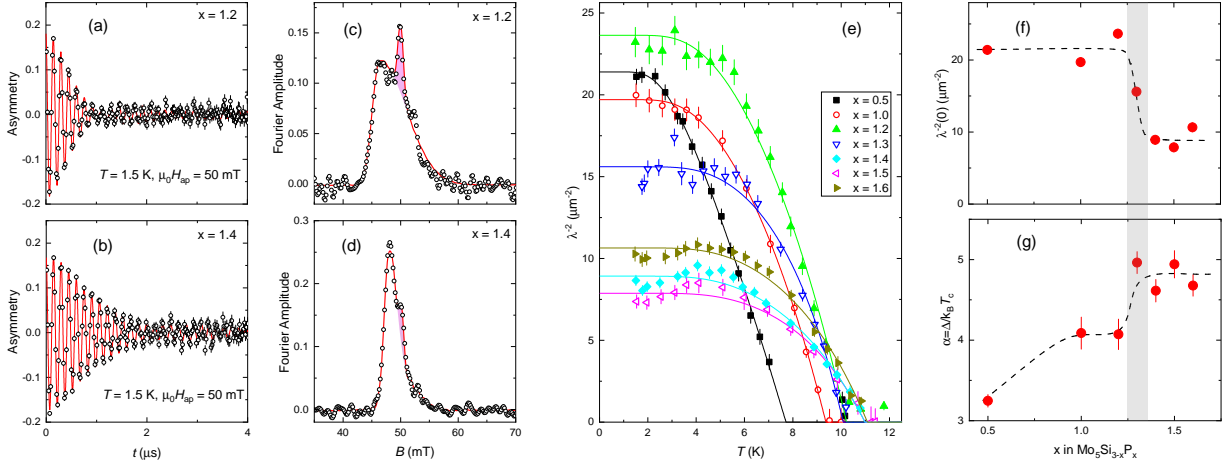


FIG. 2: (a) and (b) The muon-time spectra of $\text{Mo}_5\text{Si}_{3-x}\text{P}_x$ ($x = 1.2$ and 1.4) samples measured at $T = 1.5$ K and $\mu_0 H_{\text{ap}} = 50$ mT. The solid lines are fits of Eq. 3 to the data. (c) and (d) The Fourier transforms of asymmetry spectra presented in panels (a) and (b). Red peaks denote the background contribution originating from muons missing the sample. (e) Temperature evolution of λ^{-2} . The solid lines are fits of Eq. 3 to the data. (f) Doping dependence of $\lambda^{-2}(0)$. (g) Doping dependence of the gap to T_c ratio $\alpha = \Delta/k_B T_c$. The lines in (f) and (g) are guides for the eye. The grey stripe represents the region of an abrupt change of $\lambda^{-2}(0)$ and α .

ric $P(B)$ distribution within the FLL.^{25,26} The second central moment of the sample contribution $\langle \Delta B^2 \rangle_s$ was obtained from the fitted σ_+ and σ_- values.²⁵ The inverse squared magnetic penetration depth was further calculated as $\lambda^{-2} [\mu\text{m}^{-2}] = 9.32 \times \sqrt{\langle \Delta B^2 \rangle_s - \sigma_{\text{nm}}^2} [\mu\text{s}^{-1}]$.^{21,26} Here σ_{nm} is the nuclear moment contribution which is determined from the measurements above T_c .^{19,26}

The temperature dependencies of the inverse squared magnetic penetration depth of $\text{Mo}_5\text{Si}_{3-x}\text{P}_x$ samples are presented in Fig. 2 (e). For all dopings $\lambda^{-2}(T)$'s demonstrate saturation for $T \lesssim 4$ K (*i.e.* for temperature below $\sim 1/3$ of T_c), which is consistent with the formation of a fully gapped state. The solid lines represent best fits within the s -wave BCS model:²⁷

$$\frac{\lambda^{-2}(T)}{\lambda^{-2}(0)} = 1 + 2 \int_{\Delta(T, \varphi)}^{\infty} \left(\frac{\partial f}{\partial E} \right) \frac{E dE d\varphi}{\sqrt{E^2 - \Delta(T)^2}}. \quad (3)$$

Here $f = [1 + \exp(E/k_B T)]^{-1}$ is the Fermi function and $\Delta(T) = \Delta(0) \tanh\{1.82[1.018(T_c/T - 1)]^{0.51}\}$ is the temperature dependent superconducting gap.²⁸ $\lambda^{-2}(0)$ and $\Delta(0)$ are the zero-temperature values of the inverse squared penetration depth and the superconducting gap, respectively. The dependencies of the fit parameters, namely $\lambda^{-2}(0)$ and $\alpha = \Delta(0)/k_B T_c$ on the phosphorus content x are summarized in Figs. 2 (f) and (g), respectively. A step-like change of both parameters at $x \simeq 1.3$ is clearly visible.

The results obtained in resistivity (Fig. 1) and TF- μ SR (Fig. 2) experiments imply that the major superconducting quantities, namely the transition temperature T_c , the upper critical field H_{c2} , the magnetic penetration depth λ , and the energy gap $\Delta(0)$ demonstrate an abrupt change at $x \simeq 1.3$. Two possible scenarios can be considered. The first one assumes a formation of a competing

ordered state, where part of the carriers are gapped due to competing interactions and, therefore, become inaccessible for the Cooper pair formation. As an example of such states, one may refer to the charge-density wave (CDW) or spin-density wave (SDW) type of orders, which are widely detected for cuprate, kagome, and Fe-based superconducting families.²⁹⁻³⁷ This scenario is not plausible here, since: (i) The specific heat experiments reveal the absence of an abrupt change of the density of states at the Fermi level $[N(E_F)]$ in the vicinity of $x \simeq 1.3$.¹⁵ (ii) The zero-field μ SR experiments do not detect any kind of magnetism,¹⁵ thus implying that the SDW type of order does not come into play. (iii) The resistivity experiments reported in Ref. 14 do not detect any features at the normal-state resistivity curves up to $T \simeq 300$ K.

The second scenario assumes an emergence of flat bands at the Fermi level. In order to demonstrate this, the set of band structure calculations of $\text{Mo}_5\text{Si}_{3-x}\text{P}_x$, with a special attention paid to the critical doping region at $x \simeq 1.3$, was performed. The results are presented in Fig. 3. The shape of the first Brillouin zone and positions of the high symmetry points (Γ , X , M , N , and P) are shown in Fig. 3 (a). The major feature of the electronic structure is the band denoted by the red color, which has a substantial flattened portion. At zero doping, the flat dispersion sets at energy $\simeq 0.25$ eV above the Fermi energy (E_F), Fig. 3 (b). With increasing the phosphorus content x , E_F shifts to the higher energies and at $x \simeq 1.3$ the flat band dispersion approaches the Fermi level, Fig. 3 (e). This clearly indicates that the transition from the purely steep band to the steep band/flat band scenario is *realised* in $\text{Mo}_5\text{Si}_{3-x}\text{P}_x$. It is also remarkable that the doping level, at which the flat band approaches E_F , coincides with that, where the abrupt changes of various superconducting quantities take place

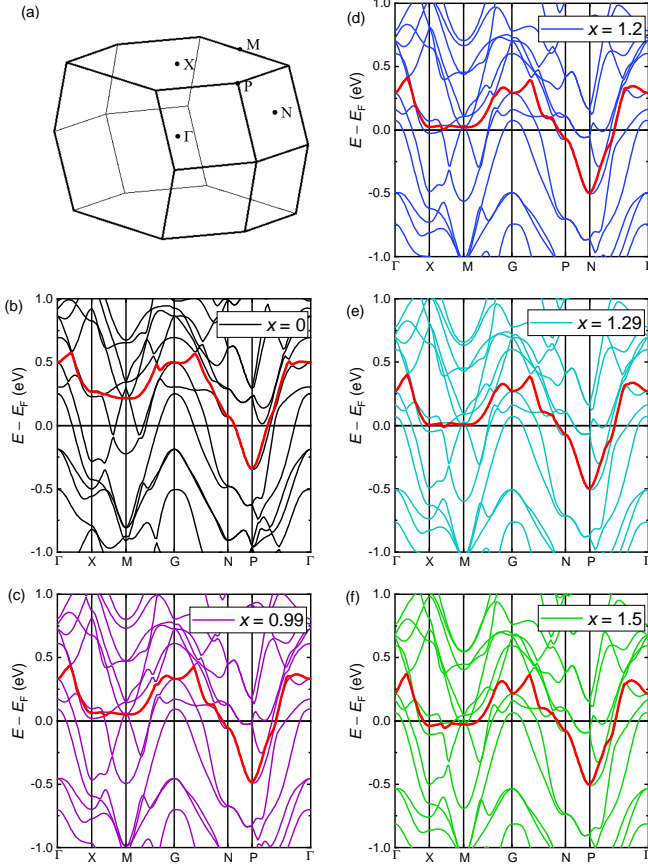


FIG. 3: (a) Brillouin zone of $\text{Mo}_5\text{Si}_{3-x}\text{P}_x$. The high-symmetry points are labeled as Γ , X, M, N, and P. (b)-(f) The electronic band structures of $\text{Mo}_5\text{Si}_{3-x}\text{P}_x$ with $x = 0.0$, 0.99, 1.2, 1.29, and 1.5. The band with extended flattened portion is denoted by the red color.

[Figs. 1 (d), 1 (e), 2 (f), and 2(g)].

The effects of band flattening on the two fundamental superconducting length scales, namely the magnetic penetration depth λ (which defines a distance for magnetic field decay) and coherence length ξ (which determines dimensions of the Cooper pairs), might be understood in relation with the corresponding changes of the Fermi velocity v_F . Note that all these quantities are obtainable from the above presented data: the value of ξ could be calculated from the measured H_{c2} by using the Ginzburg-Landau expression $H_{c2} = \Phi_0/2\pi\xi^2$,³⁸ λ is measured directly in TF- μ SR experiments, while the Fermi velocities might be estimated from the electronic structure as the first derivative of the band dispersions at E_F .

For a single-band superconductor and within the conventional BCS scenario the zero-temperature values of the coherence length and the penetration depth follow the well-known relations:

$$\xi(0) = \frac{\hbar\langle v_F \rangle}{\pi\Delta(0)} = \frac{1}{\pi\alpha} \frac{\hbar\langle v_F \rangle}{k_B T_c} \quad (4)$$

and

$$\lambda(0) = \sqrt{\frac{m^*}{\mu_0 n_s e^2}} = \sqrt{\frac{\hbar\langle k_F \rangle}{\langle v_F \rangle n_s e^2}} \quad (5)$$

Here \hbar is the reduced Planck constant, $\langle v_F \rangle$ is the average value of the Fermi velocity, n_s is the charge carrier concentration, $m^* = \hbar\langle k_F \rangle / \langle v_F \rangle$ is the effective carrier mass and $\langle k_F \rangle$ is the averaged Fermi wave vector. By hav-

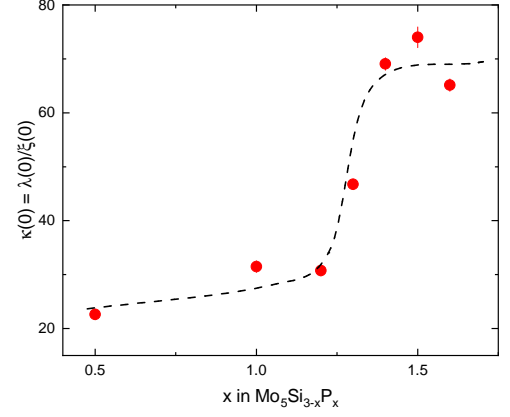


FIG. 4: The dependence of the Ginzburg-Landau parameter $\kappa = \lambda(0)/\xi(0)$ of $\text{Mo}_5\text{Si}_{3-x}\text{P}_x$ on the phosphorus content x .

ing only limited validity for $\text{Mo}_5\text{Si}_{3-x}\text{P}_x$, which is definitively not a single-band, but a multi-band superconductor [see Fig. 3], the above equations allow to capture the main features of our experimental observation: (i) The emergence of flat bands at the Fermi level, occurring at $x \gtrsim 1.3$ [Fig. 3 (d)], leads to a sudden decrease of $\langle v_F \rangle$. Following Eqs. 4 and 5, this requires the coherence length $\xi(0)$ to increase, and $\lambda(0)$ to decrease accordingly. The corresponding effects on the measured quantities $H_{c2}(0)$ and $\lambda^{-2}(0)$ are just opposed to that of $\xi(0)$ and $\lambda(0)$, in agreement with the experimental observations [Figs. 1 (e) and 2 (f)]. (ii) An opposed band flattening effect on $\xi(0)$ and $\lambda(0)$ would imply a strong change of the Ginzburg-Landau parameter $\kappa = \lambda/\xi$. This is demonstrated in Fig. 4, where $\kappa(0)$ increases by nearly three times from $\simeq 25$ for $x \leq 1.2$ to $\simeq 70$ for $x \geq 1.4$.

To conclude, the first-principles calculations and the measurements of the magnetic penetration depths, the upper critical field and the specific heat for newly discovered superconductor family $\text{Mo}_5\text{Si}_{3-x}\text{P}_x$ were conducted. The emergence of flat bands for the phosphorus content x exceeding $\simeq 1.3$ leads to an abrupt change of nearly all superconducting quantities. In particular, the transition temperature T_c increases by $\simeq 15\%$: from $\simeq 9.5$ to nearly 11 K, the upper critical field H_{c2} is more than doubles: from $\simeq 7$ to $\simeq 16$ T, while the inverse squared penetration depth (which is normally considered to be a measure of the supercarrier concentration) decreases by more than twice: from $\simeq 22$ to $\simeq 9 \mu\text{m}^{-2}$. Our results suggests that the $\text{Mo}_5\text{Si}_{3-x}\text{P}_x$ superconducting family become a unique system with easily accessible interplay between

the steep band and the steep band/flat band physics. The high transition temperatures and moderate critical fields makes this system ideal for understanding the role played by band flattening in the superconducting mechanism.

Z.G. acknowledges support from the Swiss National

Science Foundation (SNSF) through SNSF Starting Grant (No. TMSGI2_211750). Z.R. acknowledges supports from the National Key Research and Development Program of China (Grant Nos. 2018YFA0704200 and 2021YFA1401800) and the National Natural Science Foundation of China (Grant No. 12074414).

-
- * Electronic address: rustem.khasanov@psi.ch
† Electronic address: bbruan@mail.ustc.edu.cn
- ¹ R. B. Laughlin, *Anomalous Quantum Hall Effect: An Incompressible Quantum Fluid with Fractionally Charged Excitations*, Phys. Rev. Lett. **50**, 1395 (1983).
<https://doi.org/10.1103/PhysRevLett.50.1395>
 - ² V.J. Goldman and B.Su, *Resonant Tunneling in the Quantum Hall Regime: Measurement of Fractional Charge*, Science **267**, 1010 (1995).
<https://doi.org/10.1126/science.267.5200.1010>
 - ³ L. Saminadayar, D. C. Glatthli, Y. Jin, and B. Etienne, *Observation of the $e/3$ Fractionally Charged Laughlin Quasiparticle*, Phys. Rev. Lett. **79**, 2526 (1997).
<https://doi.org/10.1103/PhysRevLett.79.2526>
 - ⁴ R. de-Picciotto, M. Reznikov, M. Heiblum, V. Umansky, G. Bunin, and D. Mahalu, *Direct observation of a fractional charge*, Nature **389**, 162 (1997).
<https://doi.org/10.1038/38241>
 - ⁵ Yuan Cao, Valla Fatemi, Ahmet Demir, Shiang Fang, Spencer L. Tomarken, Jason Y. Luo, J. D. Sanchez-Yamagishi, K. Watanabe, T. Taniguchi, E. Kaxiras, R. C. Ashoori, P. Jarillo-Herrero, *Correlated Insulator Behaviour at Half-Filling in Magic Angle Graphene Superlattices*, Nature **556** 80 (2018).
<https://doi.org/10.1038/nature26154>
 - ⁶ R. Bistritzer, A.H. MacDonald, *Moire bands in twisted double-layer graphene*, PNAS **108**, 12233 (2011).
<https://doi.org/10.1073/pnas.1108174108>
 - ⁷ Xiaobo Lu, Petr Stepanov, Wei Yang, Ming Xie, Mohammed Ali Aamir, Ipsita Das, Carles Urgell, Kenji Watanabe, Takashi Taniguchi, Guangyu Zhang, Adrian Bachtold, Allan H. MacDonald, Dmitri K. Efetov, *Superconductors, Orbital Magnets, and Correlated States in Magic Angle Bilayer Graphene*, Nature **574**, 653 (2019).
<https://doi.org/10.1038/s41586-019-1695-0>
 - ⁸ Nicolas Regnault, Yuanfeng Xu, Ming-Rui Li, Da-Shuai Ma, Milena Jovanovic, Ali Yazdani, Stuart S. P. Parkin, Claudia Felser, Leslie M. Schoop, N. Phuan Ong, Robert J. Cava, Luis Elcoro, Zhi-Da Song, and B. Andrei Bernevig, *Catalogue of flat-band stoichiometric materials*. Nature volume **603**, 824 (2022).
<https://doi.org/10.1038/s41586-022-04519-1>
 - ⁹ N. B. Kopnin, T. T. Heikkilä, and G. E. Volovik, *High-temperature surface superconductivity in topological flat-band systems*, Phys. Rev. B **83**, 220503 (2011).
<https://doi.org/10.1103/PhysRevB.83.220503>
 - ¹⁰ Atousa Ghanbari, Eirik Erlandsen, Asle Sudbø, and Jacob Linder, *Going beyond the Chandrasekhar-Clogston limit in a flatband superconductor*, Phys. Rev. B **105**, L060501 (2022).
<https://doi.org/10.1103/PhysRevB.105.L060501>
 - ¹¹ V. R. Shaginyan, A. Z. Msezane, M. Ya. Amusia, and G. S. Japaridze, *Effect of superconductivity on the shape of flat bands*, Europhysics Lett. **138**, 16004 (2022).
DOI 10.1209/0295-5075/ac64ba
 - ¹² Haidong Tian, Xueshi Gao, Yuxin Zhang, Shi Che, Tianyi Xu, Patrick Cheung, Kenji Watanabe, Takashi Taniguchi, Mohit Randeria, Fan Zhang, Chun Ning Lau, and Marc W. Bockrath, *Evidence for Dirac flat band superconductivity enabled by quantum geometry*, Nature **614**, 440 (2023).
<https://doi.org/10.1038/s41586-022-05576-2>
 - ¹³ Annette Bussmann-Holder, Hugo Keller, Arndt Simon, Antonio Bianconi, *Multi-Band Superconductivity and the Steep Band – Flat Band Scenario*, Condensed Matter **4**, 91 (2019).
<https://doi.org/10.3390/condmat4040091>
 - ¹⁴ Bin-Bin Ruan, Jun-Nan Sun, Yin Chen, Qing-Song Yang, Kang Zhao, Meng-Hu Zhou, Ya-Dong Gu, Ming-Wei Ma, Gen-Fu Chen, Lei Shan, Zhi-An Ren, *Strong-coupling superconductivity with $T_c \sim 10.8$ K induced by P doping in the topological semimetal Mo_5Si_3* . Sci. China Mater. **65**, 3125 (2022).
<https://doi.org/10.1007/s40843-022-2102-8>
 - ¹⁵ The Supplemental Part contains detailed information on the methods, resistivity, specific heat, and the transverse field and zero-field μ SR experiments.
 - ¹⁶ Paolo Giannozzi, Stefano Baroni, Nicola Bonini, Matteo Calandra, Roberto Car, Carlo Cavazzoni, Davide Ceresoli, Guido L. Chiarotti, Matteo Cococcioni, and Ismaila Dabo, *QUANTUM ESPRESSO: a modular and open-source software project for quantum simulations of materials*. J Phys: Condens Matter **21** 395502 (2009).
<https://doi.org/10.1088/0953-8984/21/39/395502>
 - ¹⁷ A. Amato, H. Luetkens, K. Sedlak, A. Stoykov, R. Scheuermann, M. Elender, A. Raselli, and D. Graf, *The new versatile general purpose surface-muon instrument (GPS) based on silicon photomultipliers for μ SR measurements on a continuous-wave beam*. Rev. Sci. Instrum. **88**, 093301 (2017).
<https://doi.org/10.1063/1.4986045>
 - ¹⁸ A. Suter and B. M. Wojek, *Musrfit: A Free Platform-Independent Framework for μ SR Data Analysis*, Phys. Procedia **30**, 69 (2012).
<https://doi.org/10.1016/j.phpro.2012.04.042>
 - ¹⁹ A. Maisuradze, R. Khasanov, A. Shengelaya, and H. Keller, *Comparison of different methods for analyzing μ SR line shapes in the vortex state of type-II superconductors*, J. Phys.: Condens. Matter **21**, 075701 (2009).
<https://doi.org/10.1088/0953-8984/21/7/075701>
 - ²⁰ E. H. Brandt, *Flux distribution and penetration depth measured by muon spin rotation in high- T_c superconductors*, Phys. Rev. B **37**, 2349(R) (1988).
<https://doi.org/10.1103/PhysRevB.37.2349>
 - ²¹ E. H. Brandt, *Properties of the ideal Ginzburg-Landau vortex lattice*. Phys. Rev. B **68**, 054506 (2003).
<https://doi.org/10.1103/PhysRevB.68.054506>

- ²² B. T. Matthias, E. Corenzwit, and C. E. Miller, *Superconducting compounds*, Phys. Rev. **93**, 1415 (1954).
<https://doi.org/10.1103/PhysRev.93.1415>
- ²³ R. D. Blaugher, J. K. Hulm, and P. N. Yocom, *Superconducting phosphides of the transition metals*, J. Phys. Chem. Solids **26**, 2037 (1965).
[https://doi.org/10.1016/0022-3697\(65\)90241-6](https://doi.org/10.1016/0022-3697(65)90241-6)
- ²⁴ T. Shang, J. Philippe, J. A. T. Verezhak, Z. Guguchia, J. Z. Zhao, L.-J. Chang, M. K. Lee, D. J. Gawryluk, E. Pomjakushina, M. Shi, M. Medarde, H.-R. Ott, T. Shiroka, *Nodeless superconductivity and preserved time-reversal symmetry in the noncentrosymmetric Mo_3P superconductor*, Phys. Rev. B **99**, 184513 (2019).
<https://doi.org/10.1103/PhysRevB.99.184513>
- ²⁵ A. Suter, internal PSI report (unpublished).
- ²⁶ Rustem Khasanov, Huaxue Zhou, Alex Amato, Zurab Guguchia, Elvezio Morenzoni, Xiaoli Dong, Guangming Zhang, and Zhongxian Zhao, *Proximity-induced superconductivity within the insulating ($Li_{0.84}Fe_{0.16}$)OH layers in ($Li_{0.84}Fe_{0.16}$)OHFe_{0.98}Se*. Phys. Rev. B **93**, 224512 (2016).
<https://doi.org/10.1103/PhysRevB.93.224512>
- ²⁷ M. Tinkham, *Introduction to Superconductivity* (Krieger Publishing company, Malabar, Florida, 1975).
- ²⁸ R. Khasanov, A. Shengelaya, A. Maisuradze, F. La Mattina, A. Bussmann-Holder, H. Keller, and K.A. Müller, *Experimental evidence for two gaps in the high-temperature $La_{1.83}Sr_{0.17}CuO_4$ Superconductor*, Phys. Rev. Lett. **98**, 057007 (2007).
<https://doi.org/10.1103/PhysRevLett.98.057007>
- ²⁹ Eduardo Fradkin, Steven A. Kivelson, and John M. Tranquada, Colloquium: Theory of intertwined orders in high temperature superconductors, Rev. Mod. Phys. **87**, 457 (2015).
<https://doi.org/10.1103/RevModPhys.87.457>
- ³⁰ Tao Wu, Hadrien Mayaffre, Steffen Krämer, Mladen Horvatić, Claude Berthier, W. N. Hardy, Ruixing Liang, D. A. Bonn, and Marc-Henri Julien, *Magnetic-field-induced charge-stripe order in the hightemperature superconductor $YBa_2Cu_3O_y$* , Nature **477**, 191 (2011).
<https://doi.org/10.1038/nature10345>
- ³¹ R. M. Fernandes, A. V. Chubukov, and J. Schmalian, *What drives nematic order in iron-based superconductors?* Nature Phys. **10**, 97 (2014).
<https://doi.org/10.1038/nphys2877>
- ³² Pengcheng Dai, *Antiferromagnetic order and spin dynamics in iron-based superconductors*, Rev. Mod. Phys. **87**, 855 (2015).
DOI:<https://doi.org/10.1103/RevModPhys.87.855>
- ³³ Titus Neupert, M. Michael Denner, Jia-Xin Yin, Ronny Thomale, and M. Zahid Hasan, *Charge order and superconductivity in kagome materials*, Nat. Phys. **18**, 137 (2022).
<https://doi.org/10.1038/s41567-021-01404-y>
- ³⁴ Ritu Gupta, Debarchan Das, Charles Mielke III, Ethan T. Ritz, Fabian Hotz, Qiangwei Yin, Zhijun Tu, Chunsheng Gong, Hechang Lei, Turan Birol, Rafael M. Fernandes, Zurab Guguchia, Hubertus Luetkens, and Rustem Khasanov, *Two types of charge order with distinct interplay with superconductivity in the kagome material CsV_3Sb_5* , Commun. Phys. **5**, 232 (2022).
<https://doi.org/10.1038/s42005-022-01011-0>
- ³⁵ C. Mielke III, D. Das, J.-X. Yin, H. Liu, R. Gupta, Y.-X. Jiang, M. Medarde, X. Wu, H. C. Lei, J. J. Chang, P. Dai, Q. Si, H. Miao, R. Thomale, T. Neupert, Y. Shi, R. Khasanov, M. Z. Hasan, H. Luetkens, and Z. Guguchia, *Time-reversal symmetry-breaking charge order in a kagome superconductor*, Nature **602**, 245 (2022).
<https://doi.org/10.1038/s41586-021-04327-z>
- ³⁶ Rustem Khasanov, Debarchan Das, Ritu Gupta, Charles Mielke, III, Matthias Elender, Qiangwei Yin, Zhijun Tu, Chunsheng Gong, Hechang Lei, Ethan T. Ritz, Rafael M. Fernandes, Turan Birol, Zurab Guguchia, and Hubertus Luetkens, *Time-reversal symmetry broken by charge order in CsV_3Sb_5* , Phys. Rev. Research **4**, 023244 (2022).
<https://doi.org/10.1103/PhysRevResearch.4.023244>
- ³⁷ Z. Guguchia, C. Mielke III, D. Das, R. Gupta, J.-X. Yin, H. Liu, Q. Yin, M. H. Christensen, Z. Tu, C. Gong, N. Shumiya, Md Shafayat Hossain, Ts. Gamsakhurdashvili, M. Elender, Pengcheng Dai, A. Amato, Y. Shi, H. C. Lei, R. M. Fernandes, M. Z. Hasan, H. Luetkens, and R. Khasanov, *Tunable unconventional kagome superconductivity in charge ordered RbV_3Sb_5 and KV_3Sb_5* , Nat. Commun. **14**, 153 (2023).
<https://doi.org/10.1038/s41467-022-35718-z>
- ³⁸ Charles Kittel, *Introduction to solid state physics*, (8th ed., New Jersey: Wiley, 2013).